Effect of synthesis method parameters on the photocatalytic activity of tungsten oxide nanoplates

Cite as: AIP Advances **11**, 095220 (2021); https://doi.org/10.1063/5.0065156
Submitted: 09 August 2021 • Accepted: 04 September 2021 • Published Online: 20 September 2021

Aiymkul Markhabayeva, Khabibulla Abdullin, Zhanar Kalkozova, et al.

Effect of synthesis method parameters on the photocatalytic activity of tungsten oxide nanoplates

Cite as: AIP Advances 11, 095220 (2021); doi: 10.1063/5.0065156
Submitted: 9 August 2021 • Accepted: 4 September 2021 •
Published Online: 20 September 2021

Aiymkul Markhabayeva,[1,a)] Khabibulla Abdullin,[1,2] Zhanar Kalkozova,[1,2] Shyryn Nurbolat,[1] and Nurxat Nuraje[3,4,a)]

AFFILIATIONS

[1] National Nanotechnology Laboratory Open Type, Al-Farabi Kazakh National University, Almaty, Republic of Kazakhstan
[2] Institute of Applied Sciences and Information Technologies, Almaty, Republic of Kazakhstan
[3] Advanced Solar Energy Materials and System Lab, National Laboratory Astana (NLA), Nazarbayev University, Nursultan, Republic of Kazakhstan
[4] Department of Chemical and Materials Engineering, School of Engineering and Digital Science, Nazarbayev University, Nursultan, Republic of Kazakhstan

[a)] **Authors to whom correspondence should be addressed:** aiko_marx@mail.ru and nurxat.nuraje@nu.edu.kz

ABSTRACT

A simple chemical bath deposition method has been developed to study the formation of nanoplate morphology of tungsten oxide. The obtained materials were characterized by field emission scanning electron microscopy, transmission electron microscopy, x-ray diffractometry, Raman spectroscopy, and UV–vis diffuse reflectance spectroscopy. The photocatalytic activity of the resulting samples was further evaluated by degradation of Rhodamine B under light irradiation. It was found that both synthesis parameters and morphology affected the tungsten oxide photocatalytic activity. Tungsten oxide nanoplates obtained by a simple chemical bath deposition method have demonstrated a higher specific area and higher photocatalytic activity compared to the nanopowders obtained by the hydrothermal method.

I. INTRODUCTION

Today, industrial wastes, such as heavy metals and organic and inorganic compounds, are filling up water resources, which damage our ecosystem. Water treatment using photocatalysts and solar energy is a possible solution to this problem. It is even more attractive due to the fact that the sun is a free inexhaustible source plus green chemistry process. The photocatalytic degradation of organic dyes has been extensively studied using UV-active photocatalysts, such as titanium dioxide. The mechanism of dye degradation using the sun and a photocatalyst is based on the formation of photogenerated carriers that generates OH active radicals. The reason the wide gap semiconductors are being extensively investigated is that their valence band is usually much lower to produce OH radicals (2.38 vs NHE). However, 4% of the ultraviolet radiation coming from the sun gives us motivation to search for semiconductors with the ability to absorb a reasonable portion of the solar light spectrum.

WO_3 is a promising semiconductor for photocatalysts because it has suitable bandgap (~2.6 eV), good chemical stability under strong solar exposure, oxygen-evolution capability, long minority carrier diffusion length (~500 nm to 6 μm[1,2]), absorption of visible light (~12%), and low cost. It has been attracting scientific interest because of its wide applications in photochromic,[3–6] photoelectrochemical water oxidation,[7–11] gas sensing,[12–14] and electrochemical energy storage.[15–19] Moreover, the valence band of WO_3 is more positive than the water oxidation potential [E^o (OH/OH^-)], which makes it a good candidate for photo-oxidation of water. Various synthesis techniques have been developed to attain ideal optical properties of the photocatalyst via engineering its bandgap, particle size, crystal structure, and morphology. These properties lead to their high photocatalytic activity and light absorption ability. Furthermore, some synthesis approaches have successfully produced tungsten oxide nanostructures, such as nanosheets,[20–23] nanoplates,[24,25] nanorods,[26,27] and other morphologies.[28–30] Among

them, two-dimensional (2D) nanostructures provide more accessible active sites,[31] which might facilitate catalytic reactions toward chemical precursors.[32,33] Ma and co-workers[32] prepared tungsten oxide nanoplates by the topochemical method using Na_2WO_4 and HBF_4. They concluded that tungstic acid, H_2WO_4, is an important factor in the growth of the crystal. The crystal structure consists of WO_6 octahedra surrounded by four oxygen atoms, and each layer of WO_6 octahedra is connected to each other via hydrogen bonds. The formation of lamellar nanocrystals of tungsten oxide is explained by the formation of these layered structures in crystal planes of H_2WO_4 separated by water molecules along the [001] direction. Meng *et al.*[33] synthesized a flower hierarchical structure using citric acid ($C_6H_8O_7$) and found that (−COOH) functional groups are responsible for the growth of nanoplates.

Herein, we have developed a chemical bath deposition method at a relatively low temperature ~90 °C and normal atmospheric pressure to synthesize WO_3 nanoplates and compared it with a common hydrothermal synthesis method. The hydrothermal method can also be used to grow nanostructures; however, it requires high pressure and additional apparatus and there is no possibility to observe the reaction process. Despite that the same solution was used, it was found that the synthesis temperature or atmospheric conditions strongly influenced the growth of crystals and their final morphology in both cases. Furthermore, the synthesis at normal atmospheric pressure and at a temperature of ~90 °C produced thinner nanoplates, relative to the synthesis by the hydrothermal (pressure above atmospheric) technique at 180 °C. It is known that enlarged surface area associated with thin thickness is beneficial to obtain better light scattering and charge transportation. Accordingly, it is very important to investigate the correlation of the photocatalyst's morphology with the light absorption and the photocatalytic activity.

Therefore, in this research, we mainly studied the formation of WO_3 nanoplates at ambient pressure and relatively low temperature and also investigated their photocatalytic activity in parallel with the WO_3 nanoplates synthesized by the hydrothermal approach through conducting the light degradation experiment of Rhodamine B.

II. MATERIALS AND METHODS

A. Chemicals and materials

Sodium tungstate dihydrate (Sigma-Aldrich, >99%), hydrochloric acid (Acros Organics, 98%), and citric acid (Acros Organics, 98%) were used as starting materials for the synthesis of tungsten oxides.

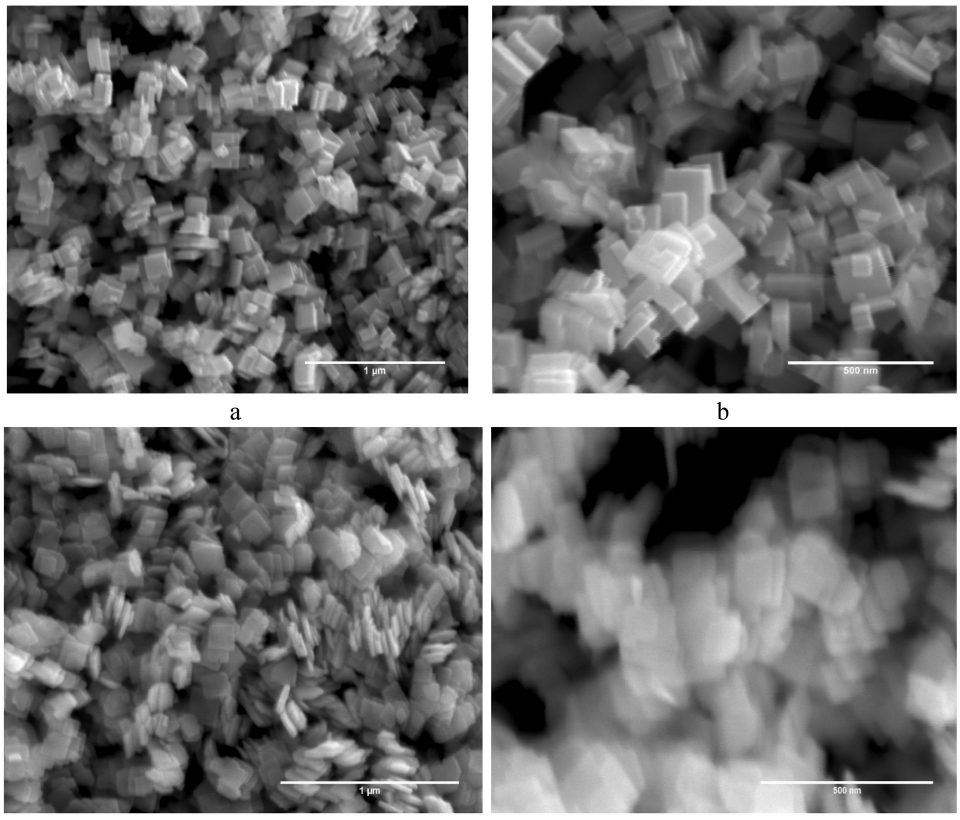

FIG. 1. SEM images of WO180 (a) and (b) and WO90 nanoplates (c) and (d).

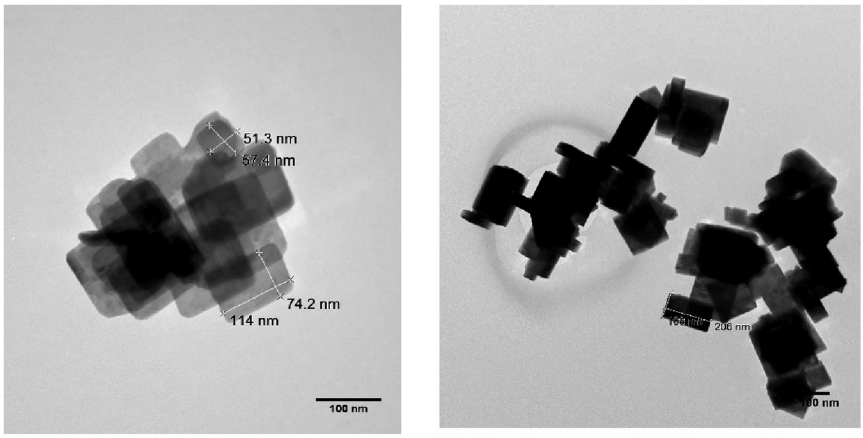

FIG. 2. TEM images of WO90 (a) and WO180 (b) nanoplates.

B. Synthesis of WO_3 nanoplates

Tungsten oxide nanopowders were synthesized from precursor solution of 0.1M sodium tungstate ($Na_2WO_4 * 2H_2O$) and 0.1M citric acid. The solution was stirred at room temperature for an hour. Then, 5M solution of hydrochloric acid was added dropwise to reach the acidity level to pH = 1.5. The synthesis was carried out in two ways: in the first case, the synthesis by the chemical bath deposition method took place in a beaker placed on a magnetic stirrer with heating at a temperature of ~90 °C for 1 h (labeled as WO90). In the second case (hydrothermal synthesis method), the same precursors were used. The yellow solution was transferred to a Teflon-lined stainless-steel autoclave (50 ml) reactor to synthesize at a higher temperature of 180 °C for 4 h (labeled as WO180). The resulting solution was cooled to room temperature, and yellow powder products were washed with water and ethanol several times. The samples were dried at 90 °C in air for about 12 h. Additional thermal annealing was carried out in a muffle furnace (SNOL 8.2/1100) at 400 °C to obtain a polycrystalline phase of tungsten oxide nanopowders.

C. Analysis and methods

The crystal phase composition and crystallinity of the prepared products were characterized by using an x-ray diffractometer (Rigaku Ultima III and MiniFlex Rigaku). X-ray diffraction patterns were obtained by scanning the 2θ range from 5 to 90°, step size = 0.02°, and scan time at 0.33 min/deg. The x-ray source used was an x-ray tube (a copper anode, CuKα radiation) at a wavelength of 1.5418 Å, voltage of 40 kV, and current of 44 mA. Raman spectra were measured on an NTegra Spectra (NT-MDT) instrument using a blue laser at a wavelength of 473 nm. The irradiation time of the samples with a laser source was 30 s, and the spot diameter (from the laser) on the sample was ~2 μm. At 100% intensity, the laser power was 35 mW. The SEM images presented in this work were obtained using a Hitachi S4300 E/N FE-SEM. The TEM images were obtained using a Hitachi H-9500 transmission electron microscope; the accelerating voltage was varied in the range of 150–200 kV. Diffuse reflectance spectra of the samples were measured using a Cary

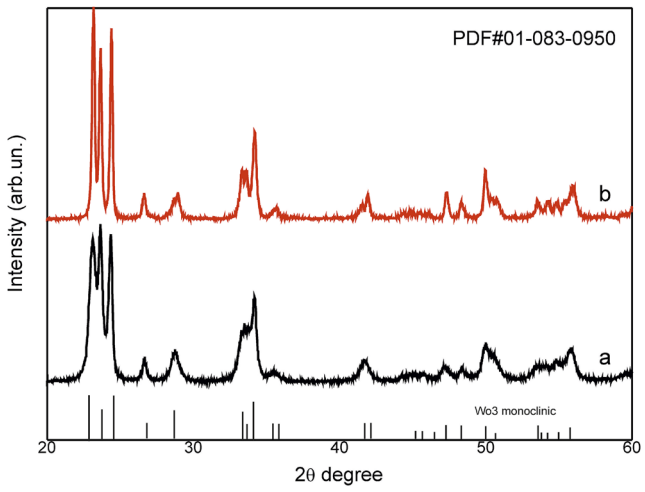

FIG. 3. XRD of WO90 (a) and WO180 (b) nanoplates.

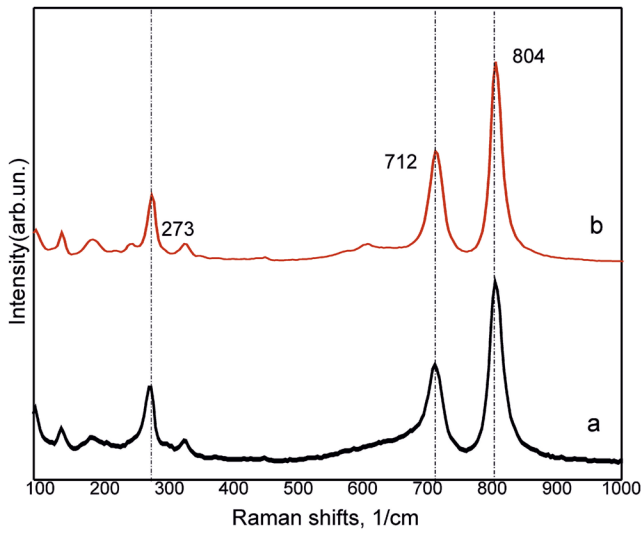

FIG. 4. Raman spectra of WO90 (a) and WO180 (b) nanoplates.

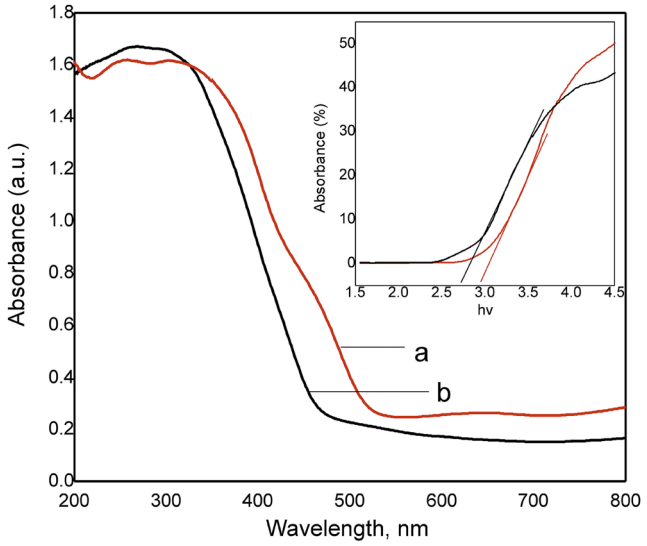

FIG. 5. UV–vis absorption spectra of WO90 (a) and WO180 (b) nanoplates.

5000 UV-Vis-NIR spectrophotometer equipped with an integrating sphere.

The photocatalytic activity of WO_3 nanoplates was evaluated by the process of photodegradation of Rhodamine B. UV light was obtained using a 14 W mercury lamp, and the average light intensity was 100 mW cm^{-2}. 125 ml of Rhodamine B solution containing a certain amount of the test sample (5 mg) was treated in an ultrasonic bath for 30 min and stirred at room temperature in the dark until an equilibrium was established. Then, the solution with the dye and powder was exposed to light. The concentration of Rhodamine B (RhB) dye at different irradiation times was measured using a Lambda 35 optical spectrophotometer at absorption maxima of 554 nm.

III. RESULTS AND DISCUSSION

Figure 1 shows SEM images of the synthesized tungsten oxide nanopowders. As shown in Fig. 1, uniform square and rectangular nanoplates are observed in both cases but the thickness of nanoplates synthesized at 90 °C is less than that of nanoplates synthesized at 180 °C (Fig. 1). The sizes of WO_3 nanoplates synthesized at ~180 °C in x- and y-directions range from 50 to 200 nm. Their thickness is ~50 nm. However, the size of the nanoplates synthesized at 90 °C in two directions is in the range of 50–150 nm and their thickness is greater than 20 nm (Fig. 2). Although we cannot accurately determine the thickness, it can be roughly estimated from its contrast, where lighter contrast indicates thinner thickness in the TEM image (Fig. 2).[34]

Figure 3 shows x-ray diffraction patterns of WO_3 nanoplates. It can be seen that the nanoplates obtained by the two methods do not differ in structure and their XRD data coincide with the JCPDS No-01-083-0950 standard for the monoclinic modification of tungsten oxide. There is a difference in peak FWHM when comparing the XRD data of the samples. This is due to different crystallite sizes.

Raman spectra of WO_3 nanoplates synthesized at ~90 and 180 °C are shown in Fig. 4. The main vibrational modes for the WO_3 lattice are stretching vibrations with a change in bond lengths (ν), bending vibrations with changing angles between bonds–planar (δ), and out-of-plane (γ). It is known that these modes of tungsten oxide are ~807, ~716, and ~271 cm^{-1}, which correspond to the stretching of O–W–O and W–O, and the bending of O–W–O.[35] A group of weak peaks below 200 cm^{-1} correspond to the lattice vibration, and the sharp peaks at about 270 and 330 cm^{-1} correspond to bending strain δ (O–W–O).[36] A slight red shift in comparison with the literature can be associated with the small size of the obtained nanopowders. Raman spectra also show the identical structure of the obtained nanopowders.

Light absorption and optical bandgap of photocatalysts are important parameters. UV–vis diffuse reflectance spectra of nanoplates are shown in Fig. 5. The inset graph shows the Kubelka–Munk function plotted against photon energy. The optical

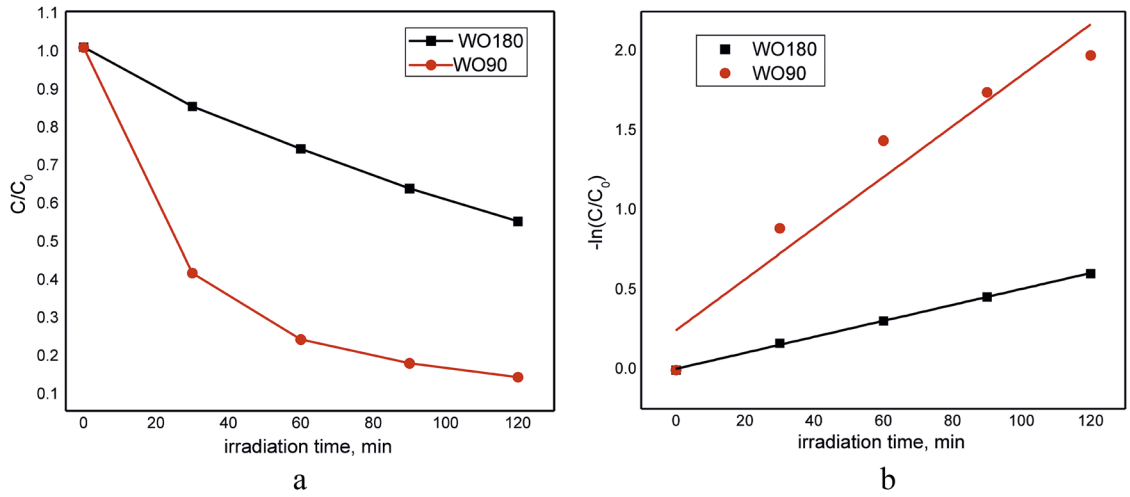

FIG. 6. Degradation curves of RhB containing WO90 and WO180 nanoplates under light illumination for 2 h (a) and ln (C/C_0) vs irradiation time plots (b).

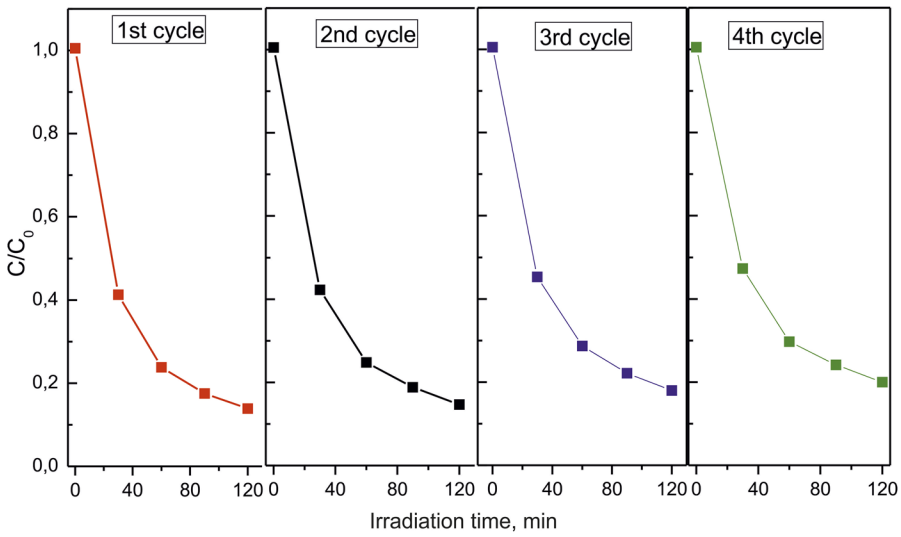

FIG. 7. Photocatalytic oxidation of Rhodamine B aqueous solution containing WO90 nanoplates by repeating four cycles.

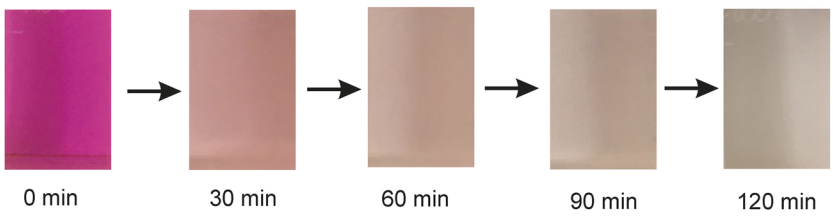

FIG. 8. Decolorization of Rhodamine B aqueous solution containing WO90 nanoplates under light irradiation.

bandgap of nanopowders is estimated using the following equation:

$$\alpha h\nu = A(h\nu - E_g)^n,$$

where α is the absorption coefficient and E_g is optical bandgap of the semiconductor. A is a constant, and n is 2 for an allowed indirect transition or ½ for direct transition. Transition is indirect for WO_3, so $(\alpha h\nu)^{1/2}$ is plotted as a function of photon energy. The bandgap is estimated to be 2.6 and 2.8 for WO90 and WO180 nanoplates, respectively.

The photocatalytic activity of the obtained nanoplates was estimated in the oxidation reaction of the organic dye Rhodamine B. Figure 6(a) shows a comparison of the kinetic curves of the photocatalytic oxidation of RhB aqueous solution containing WO90 and WO180 nanoplates. As can be seen from Fig. 6(a), WO90 nanoplates have a relatively high photocatalytic activity. Figure 6(b) shows the correlation between Ln (C/C_0) and irradiation time. The rate constant, k, for decomposition of RhB was calculated using Langmuir–Hinshelwood kinetics. Both 0.03 and 0.005 min^{-1} were obtained for WO90 and WO180 nanoplates, respectively. WO90 demonstrated higher adsorption and photocatalytic activity.

The stability of photocatalysts is an important factor in water purification. Many semiconductors undergo photocorrosion, are unstable in aqueous media, and lose their photocatalytic activity over time when they are exposed to light. Therefore, we examined the stability of photocatalyst WO90 nanoplates. A certain amount of photocatalysts was filtered after every cycle, and fresh Rhodamine B solution was used to test stability. Figure 7 shows that the obtained WO90 nanoplates have good stability, and the real photo of color degradation of the Rhodamine B solution demonstrated high photocatalytic activity of samples (Fig. 8).

IV. CONCLUSION

Highly photoactive WO_3 thin nanoplates have been successfully synthesized by a chemical bath deposition method. It was shown that the thickness of the WO_3 nanoplates can be controlled by synthesis parameters, such as temperature and pressure. The low temperature chemical bath deposition synthesis approach not only can grow thin square nanoplates relative to traditional hydrothermal synthesis at above 120 °C (autoclave synthesis method), but also it is relatively low cost from the economical point of view. The nanoplates produced from the chemical bath deposition approach have a higher adsorption rate constant than that of the WO_3 nanoplates synthesized at 180 °C, which might explain the high surface area of WO90. Moreover, the high photocatalytic activity of the WO90 nanoplates for degradation of organic dye RhB makes them a good candidate for application in water treatment.

ACKNOWLEDGMENTS

This research was funded by the Program of the Committee of Science of the Ministry of Education and Science of the Republic of Kazakhstan, Grant Nos. AP08956791 and AP09259253.

The authors express their special thanks to Marat Nuraje from ERMHS for editing and proof-reading the whole manuscript.

DATA AVAILABILITY

The data that support the findings of this study are available from the corresponding authors upon reasonable request.

REFERENCES

[1]R. A. Pala, A. J. Leenheer, M. Lichterman, H. A. Atwater, and N. S. Lewis, "Measurement of minority-carrier diffusion lengths using wedge-shaped semiconductor photoelectrodes," Energy Environ. Sci. **7**, 3424–3430 (2014).
[2]R. H. Coridan, K. A. Arpin, B. S. Brunschwig, P. V. Braun, and N. S. Lewis, "Photoelectrochemical behavior of hierarchically structured Si/WO_3 core-shell tandem photoanodes," Nano Lett. **14**, 2310–2317 (2014).
[3]S. Wang, W. Fan, Z. Liu, A. Yu, and X. Jiang, "Advances on tungsten oxide based photochromic materials: Strategies to improve their photochromic properties," J. Mater. Chem. C **6**, 191–212 (2018).
[4]M. Sun, N. Xu, Y. W. Cao, J. N. Yao, and E. G. Wang, "Nanocrystalline tungsten oxide thin film: Preparation, microstructure, and photochromic behavior," J. Mater. Res. **15**, 927–933 (2000).
[5]Q. Zhang, R. Wang, Y. Lu, Y. Wu, J. Yuan, and J. Liu, "Highly efficient photochromic tungsten oxide@PINPAM composite spheres with a fast response," ACS Appl. Mater. Interfaces **13**, 4220–4229 (2021).
[6]S. Wang, X. Feng, J. Yao, and L. Jiang, "Controlling wettability and photochromism in a dual-responsive tungsten oxide film," Angew. Chem. **118**, 1286–1289 (2006).
[7]Y. Liu, S. Xie, C. Liu, J. Li, X. Lu, and Y. Tong, "Facile synthesis of tungsten oxide nanostructures for efficient photoelectrochemical water oxidation," J. Power Sources **269**, 98–103 (2014).
[8]Y. Ping, Y. Li, F. Gygi, and G. Galli, "Tungsten oxide clathrates for water oxidation: A first principles study," Chem. Mater. **24**, 4252–4260 (2012).
[9]G. Zheng, J. Wang, H. Liu, V. Murugadoss, G. Zu, H. Che, C. Lai, H. Li, T. Ding, Q. Gao, and Z. Guo, "Tungsten oxide nanostructures and nanocomposites for photoelectrochemical water splitting," Nanoscale **11**, 18968–18994 (2019).
[10]Y. Shabdan, A. Markhabayeva, N. Bakranov, and N. Nuraje, "Photoactive tungsten-oxide nanomaterials for water-splitting," Nanomaterials **10**, 1871 (2020).
[11]A. A. Markhabayeva, M. Moniruddin, R. Dupre, K. A. Abdullin, and N. Nuraje, "Designing of WO_3@Co_3O_4 heterostructures to enhance photoelectrochemical performances," J. Phys. Chem. A **124**, 486–491 (2019).
[12]Y. S. Kim, "Thermal treatment effects on the material and gas-sensing properties of room-temperature tungsten oxide nanorod sensors," Sens. Actuators, B **137**, 297–304 (2009).
[13]E. Navarrete, C. Bittencourt, P. Umek, and E. Llobet, "AACVD and gas sensing properties of nickel oxide nanoparticle decorated tungsten oxide nanowires," J. Mater. Chem. C **6**, 5181–5192 (2018).
[14]T. D. Senguttuvan, V. Srivastava, J. S. Tawal, M. Mishra, S. Srivastava, and K. Jain, "Gas sensing properties of nanocrystalline tungsten oxide synthesized by acid precipitation method," Sens. Actuators, B **150**, 384–388 (2010).
[15]P. A. Shinde and S. C. Jun, "Review on recent progress in the development of tungsten oxide based electrodes for electrochemical energy storage," ChemSusChem **13**, 11–38 (2020).
[16]S. P. Gupta, H. H. Nishad, S. D. Chakane, S. W. Gosavi, D. J. Late, and P. S. Walke, "Phase transformation in tungsten oxide nanoplates as a function of post-annealing temperature and its electrochemical influence on energy storage," Nanoscale Adv. **2**, 4689–4701 (2020).
[17]J. B. Mitchell, W. C. Lo, A. Genc, J. LeBeau, and V. Augustyn, "Transition from battery to pseudocapacitor behavior via structural water in tungsten oxide," Chem. Mater. **29**, 3928–3937 (2017).
[18]X. Huo, W. Shen, R. Li, M. Zhang, and M. Guo, "A novel heterostructure of oriented core/shell tungsten oxide nanorod arrays for electrochromo-pseudocapacitor," Scr. Mater. **174**, 1–5 (2020).
[19]K. A. Abdullin, Z. K. Kalkozova, A. A. Markhabayeva, R. Dupre, M. Moniruddin, and N. Nuraje, "Core–shell (W@WO_3) nanostructure to improve electrochemical performance," ACS Appl. Energy Mater. **2**, 797–803 (2018).
[20]G. Zhang, W. Guan, H. Shen, X. Zhang, W. Fan, C. Lu, H. Bai, L. Xiao, W. Gu, and W. Shi, "Organic additives-free hydrothermal synthesis and visible-light-driven photodegradation of tetracycline of WO_3 nanosheets," Ind. Eng. Chem. Res. **53**, 5443–5450 (2014).
[21]D. Zhang, Y. Fan, G. Li, Z. Ma, X. Wang, Z. Cheng, and J. Xu, "Highly sensitive btex sensors based on hexagonal WO_3 nanosheets," Sens. Actuators, B **293**, 23–30 (2019).
[22]Z. Wang, D. Wang, and J. Sun, "Controlled synthesis of defect-rich ultrathin two-dimensional WO_3 nanosheets for NO_2 gas detection," Sens. Actuators, B **245**, 828–834 (2017).
[23]C. Wang, S. Zhang, L. Qiu, S. A. Rasaki, F. Qu, T. Thomas, Y. Liu, and M. Yang, "Ru-decorated WO_3 nanosheets for efficient xylene gas sensing application," J. Alloys Compd. **826**, 154196 (2020).
[24]D. Xue, Y. Wang, J. Cao, G. Sun, and Z. Zhang, "Improving methane gas sensing performance of flower-like SnO_2 decorated by WO_3 nanoplates," Talanta **199**, 603–611 (2019).
[25]J. Y. Zheng, G. Song, J. Hong, T. K. Van, A. U. Pawar, D. Y. Kim, C. W. Kim, Z. Haider, and Y. S. Kang, "Facile fabrication of WO_3 nanoplates thin films with dominant crystal facet of (002) for water splitting," Cryst. Growth Des. **14**, 6057–6066 (2014).
[26]J. Wang, E. Khoo, P. S. Lee, and J. Ma, "Synthesis, assembly, and electrochromic properties of uniform crystalline WO_3 nanorods," J. Phys. Chem. C **112**, 14306–14312 (2008).
[27]Z. Gu, T. Zhai, B. Gao, X. Sheng, Y. Wang, H. Fu, Y. Ma, and J. Yao, "Controllable assembly of WO_3 nanorods/nanowires into hierarchical nanostructures," J. Phys. Chem. B **110**, 23829–23836 (2006).
[28]L. Wang, A. Teleki, S. E. Pratsinis, and P. I. Gouma, "Ferroelectric WO_3 nanoparticles for acetone selective detection," Chem. Mater. **20**, 4794–4796 (2008).
[29]G. Wang, Y. Ling, H. Wang, X. Yang, C. Wang, J. Z. Zhang, and Y. Li, "Hydrogen-treated WO_3 nanoflakes show enhanced photostability," Energy Environ. Sci. **5**, 6180–6187 (2012).
[30]W. Shi, X. Zhang, J. Brillet, D. Huang, M. Li, M. Wang, and Y. Shen, "Significant enhancement of the photoelectrochemical activity of WO_3 nanoflakes by carbon quantum dots decoration," Carbon **105**, 387–393 (2016).
[31]C. Tan, X. Cao, X.-J. Wu, Q. He, J. Yang, X. Zhang, J. Chen, W. Zhao, S. Han, G.-H. Nam, M. Sindoro, and H. Zhang, "Recent advances in ultrathin two-dimensional nanomaterials," Chem. Rev. **117**, 6225–6331 (2017).
[32]J. Ma, J. Zhang, S. Wang, T. Wang, J. Lian, X. Duan, and W. Zheng, "Topochemical preparation of WO_3 nanoplates through precursor H_2WO_4 and their gas-sensing performances," J. Phys. Chem. C **115**, 18157–18163 (2011).
[33]D. Meng, G. Wang, X. San, Y. Song, Y. Shen, Y. Zhang, K. Wang, and F. Meng, "Synthesis of WO_3 flower-like hierarchical architectures and their sensing properties," J. Alloys Compd. **649**, 731–738 (2015).
[34]D. Williams and C. Carter, *Introduction to Transmission Electron Microscopy* (Plenum Press, New York, 1996).
[35]M. F. Daniel, B. Desbat, J. C. Lassegues, B. Gerand, and M. Figlarz, "Infrared and Raman study of Wo_3 tungsten trioxides and WO_3, xH_2O tungsten trioxide tydrates," J. Solid State Chem. **67**, 235–247 (1987).
[36]A. Rougier, F. Portemer, A. Quédé, and M. El Marssi, "Characterization of pulsed laser deposited WO_3 thin films for electrochromic devices," Appl. Surf. Sci. **153**, 1–9 (1999).